Investigation of temperature dependant current transport mechanism in Ag/In$_2$O$_3$/p-Si/Al heterojunction

Ashwani Kumar

Department of Physics, Government College Sujanpur (H.P.) 176110, India

A B S T R A C T

Employing the pulsed laser ablation technique nano-crystalline thin films of Indium oxide (In$_2$O$_3$) are deposited successfully on boron doped silicon substrate. The structural and morphological parameters of the films are investigated by using X-ray diffraction and atomic force microscopic (AFM) spectroscopy, respectively. The deposited films are the crystalline nanostructures with (400) as preferred diffraction peak and grain size of 56.56 nm approximately. The computed roughness (Rq) of In$_2$O$_3$ film is 1.02 nm. The AFM analysis validated the deposition of homogeneous smooth In$_2$O$_3$ films with surface roughness of the order of nanometer. *UV–vis* spectroscopy was used to study the optical properties of the films. Greater than 80% transparency in visible region was exhibited by the films. The value of the optical band gap was found to be 3.89 eV. The electrical parameters dominating the mechanism of current transport in n-In$_2$O$_3$/p-Si heterojunction were explored by observing the temperature-dependent current–voltage (*I–V*) properties. In the temperature range of 80–300 K, the ideality factor and barrier height were found to be strongly temperature dependent. It was noticed that with the decrease in temperature there is increase in ideality factor whereas decrease in barrier height which confirm the interfacial imperfections and inhomogeniety in potential barrier height distributions. The temperature dependence of *I–V* data has revealed the existence of double Gaussian distribution of barrier heights with mean values of 0.85eV and 0.78eV with standard deviation of 0.014 V and 0.012 V respectively. The modified Richardson's plot gives the average barrier height and Richardson's coefficient as 0.86eV and 4.7×10^5 Am^{-2}K^{-2} in the temperature range 300 K–180 K and 0.77eV and 5.2×10^5 Am^{-2}K^{-2}, respectively in the temperature range 160 K–80 K. The values of Richardson's constants are of the order of known theoretical value of 3.2×10^5 Am^{-2} K^{-2}.

1. Introduction

The wide band gap transparent semiconducting oxides are in great demand in basic research for the fabrication of thin film optoelectronic devices [1–3]. The bulk and surface properties of these films decide the optimum performance of the fabricated devices. In$_2$O$_3$ has band gap about 3.7eV and optical transmittance greater than 80% within the visible spectrum [4,5]. In In$_2$O$_3$ the oxygen defects also produce visible the light sensing [6]. The ultraviolet light detection is also important in flame sensors, UV photosensors, spatial optical communication devices, chemical and biological sensors, laser-based devices etc. [7].

The low electrical resistivity and high optical transparency in visible spectrum have made the In$_2$O$_3$ applicable in wide range of technological applications [8]. Moreover the direct band gap that these nanostructure thin films possess is equal to 3.94 which is much
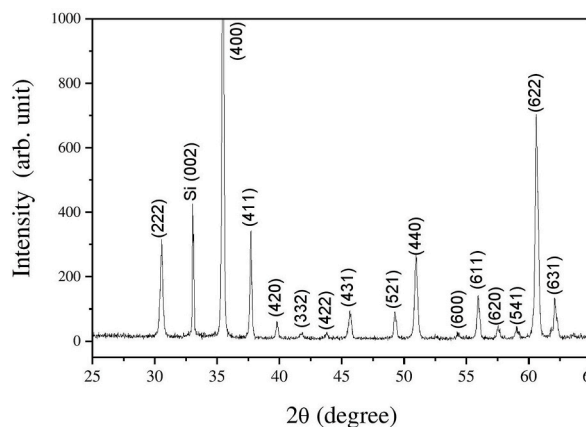
Fig. 1. X-ray diffraction spectra of In_2O_3 film deposited on p-type silicon.

greater than the bulk band gap of In_2O_3 (3.6 eV) due to the effect of quantum confinement [9,10]. Many techniques can be employed to fabricate thin films of In_2O_3 which are DC magnetron sputtering [11], radio-frequency sputtering [12], electron beam evaporation [13], high density plasma evaporation [14], thermal reactive evaporation [15], spray pyrolysis [16], sol-gel [17], chemical vapor deposition [18], and pulsed laser deposition [19] etc.

The choice of substrate; material used to form films; the thickness of the films; dopants used and the design of junction decide the associated parameters of the fabricated device and are in research for a long time period. The optoelectronic devices and diodes are fabricated by In_2O_3 thin films by several researchers. A mixture of In_2O_3 and SiO_2 acts as thick film *p-n* junction which detects the gamma radiations due to current enhancement in *I–V* characteristics [20]. For diode applications In_2O_3 films has been deposited employing various techniques by many researchers. Using sol-gel technique; Gupta et al. deposited In_2O_3 thin film [21]. In_2O_3/Si junction solar cells were prepared by novel rapid thermal oxidation (RTO) technique using halogen lamp [22]. Savarimuthu et al. have synthesized the In_2O_3 films using sol-gel spin coating technique [23]. Cheng et al. have prepared In_2O_3 nanorods with length of 120 nm and diameter of 20 nm by sol-gel technique [24]. Kaleemulla et al. deposited In_2O_3 by flash evaporation to investigate the film parameters [25]. To study the opto-electric characteristics; *p*-Si/*n*-In_2O_3 diodes were fabricated Jet Nebulizer Spray Pyrolysis (JNSP) technique [26]. By using reactive sputtering technique in oxygen atmosphere Schottky diodes on indium oxide films were fabricated which show the suitable rectification [27]. The temperature dependant *I–V* and *(C–V)* characteristics of Schottky contacts heterojunctions were studied over the wide temperature range and the Gaussian distribution of barrier height was found due non-pure thermionic emission theory [28–34].

The purpose of the present work is to fabricate Ag/In_2O_3/*p*-Si/Al heterojunction by pulsed laser abalation technique to study the structural, optical and electrical properties in wide range of temperature since In_2O_3 acts as good passivation layer in various photovoltaic devices. In this study we have studied the barrier inhomogeneities in *I–V* characteristics in detail. The various electrical parameters namely barrier height, ideality factor, activation energy, Richardson constant are also estimated. It was found that the prepared Ag/In_2O_3/*p*-Si/Al heterojunction exhibit rectifying behavior. The low temperature analysis of *I–V* parameters allow to determine the effective current transport mechanism and the affecting factors.

1.1. Experimental procedure

To fabricate Ag/In_2O_3/*p*-Si/Al heterojunction thin films of In_2O_3 were deposited on boron doped silicon wafer with (400) surface orientation using pulsed laser ablation technique. Before the deposition silicon substrate was cleaned by organic solvents and deionized water for 10 min under constant ultrasonication followed by etching in a 40% HF solution so that oxide layer can be removed and then finally rinsed with deionized water.

Now to form ohmic contacts; aluminum metal was deposited under 3×10^{-6} mbar vacuum on the back side. The pulsed laser deposition technique was used to abalate pure In_2O_3 target so that thin film can be grown on the front side of silicon substrate. The back ohmic contacts were protected by Picein coating. To ablate the In_2O_3 target we have used KrF (248 nm) COHERENT COMPLEX PRO 205 F laser at 300 mJ energy with 10 Hz repetition rate. Before the deposition 3×10^{-6} mbar pressure was maintained in the chamber. During deposition oxygen partial pressure of 7×10^{-3} mbar was maintained and the substrate to target distance was kept 5 cm. Finally, silver metal was thermally evaporated from the tungsten filament into In_2O_3 film surface through masks with circular holes of 1 mm diameter under 3×10^{-6} mbar vacuum to get the metal contacts. No energy barrier formation was detected between In_2O_3 and vacuum-deposited metal contacts [35]. The *I–V* parameters were determined by programmable Keithley 2400 source-meter in the temperature range of 80 K–300 K. An IEEE-488 interface card was used to measure the electrical parameters. X-ray diffraction pattern of thin films were obtained by using Panalytical Xpert Pro diffractometer. Non-contact mode AFM images were performed by SPM 5500 (Agilent) using closed loop scanner with non-contact low frequency silicon cantilever (force constant: 21–98 N/m). The optical measurements were performed by using PerkinElmer Lambda-750 spectrophotometer.
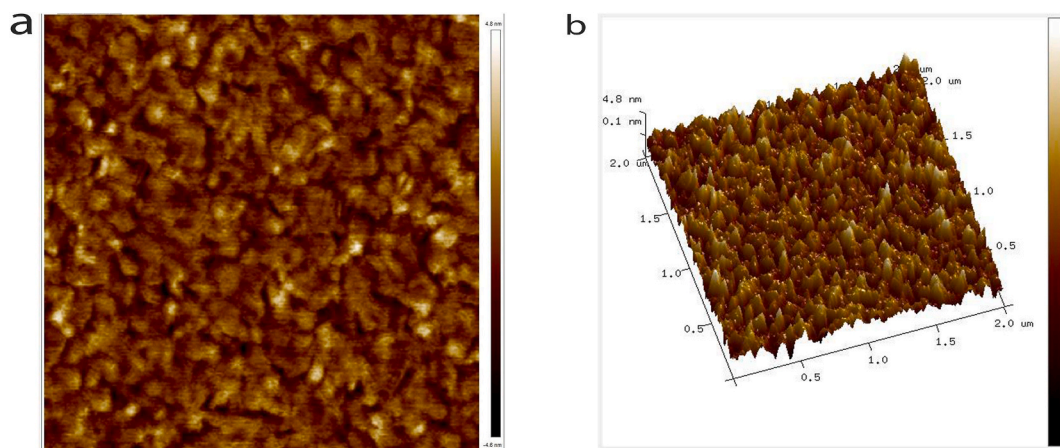
Fig. 2. (a)Atomic force microscopy 2D image of In_2O_3 thin film on *p*-type silicon.
(b)Atomic force microscopy 3D image of In_2O_3 thin film on *p*-type silicon.
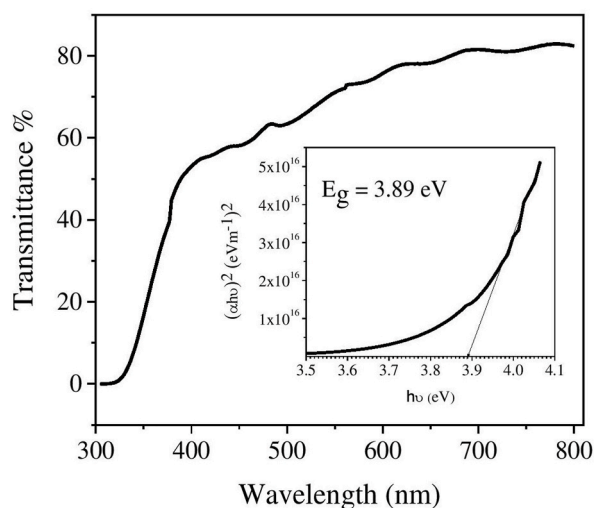

Fig. 3. Optical transmittance spectra of In_2O_3 thin films on quartz as a function of wavelength. The inset graph shows the plots of $(\alpha h\upsilon)^2$ versus photon energy ($h\upsilon$).

2. Results and discussion

2.1. XRD studies

The crystalline structure of In_2O_3 thin films deposited on Si substrate was analyzed by X-ray diffraction (XRD) spectra, as shown in Fig. 1. The peaks related to pure In_2O_3 phase were detected in the XRD spectra and no other phase was present. The cubic crystalline structure was observed in the deposited films as per JCPDS file no. 06–0416 [36]. The stronger diffraction (400) peak was shown at 2θ of $35.47°$. Among the strong peaks, there are a few minor peaks related to cubic phase, which were also observed in the films, i.e. (211), (321), (400), (521), (431), (440), (600), (611), and (620), respectively. Crystalline size calculated from (400) peak using the Scherrer formula [37] is found to be 56.56 nm for the nanostructured In_2O_3 films.

2.2. AFM studies

The growth morphology and surface quality of the prepared films can be understood by atomic force microscopy. The surface roughness of the In_2O_3 films was estimated by atomic force microscope used in non-contact mode over the film area of $10 \times 10 \ \mu m^2$. The two and three dimensional surface morphology of In_2O_3 film on *p*-type silicon is shown in Fig. 2(a) and (b); respectively. Smooth surface of the film is found to exit with uniform distribution of grains. The film with condensed columnar structures free from cracks and defects was obtained. The approximate roughness (Rq) of In_2O_3 film was found to be 1.02 nm. The AFM analysis validated the
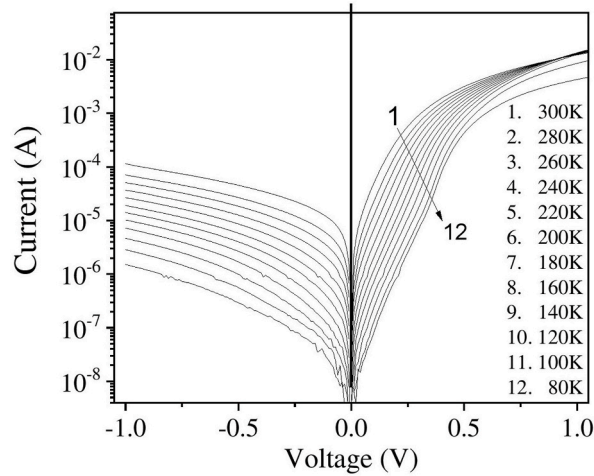
Fig. 4. Current-voltage characteristics of Ag/In$_2$O$_3$/p-Si/Al heterojunction diodes at different temperatures.

deposition of homogeneous smooth In$_2$O$_3$ films with surface roughness of the order of nanometer.

2.3. Optical band gap study

The energy band gap (E_g) of In$_2$O$_3$ films can be calculated from the absorption coefficient analysis. The numerical value of band gap can be estimated from absorption characteristics in the fundamental absorption region by the equation

$$(\alpha h \nu)^2 = A(h\nu - E_g) \tag{1}$$

where h stands for Planck's constant, α is the absorbance, ν is frequency of photon, A is constant whose value depends on the probability of transition and E_g is optical band gap. Using the *UV/VIS* spectrophotometer in the range from 250 nm to 800 nm the measurements were done to achieve the spectrum of transmission as shown in Fig. 3. The optical band gap can be measured from the sharp absorption resulting from allowed transitions. Tauc plot [38] depicted in the inset of Fig. 3 determine the absorption coefficient above the threshold limit. The optical band gap of In$_2$O$_3$ was estimated from the absorption edge obtained by extrapolating the linear portion of the plot to $\alpha = 0$ which corresponds to zero absorption. The optical band gap obtained in the present case is 3.89 eV which is in good agreement as reported in literature [39]. The nanocrystalline nature of the thin film has enhanced the value of band gap as compared to the bulk band gap of the material.

2.4. Temperature dependent I–V analysis

The *I–V* analysis of Ag/In$_2$O$_3$/p-Si/Al heterojunction depicts the asymmetry with respect to positive and negative biasing at different temperatures as shown in Fig. 4. At 300 K about two orders rectification ratio was obtained at ± 1 V. From the inspection of plots a linear region was found in the intermediate range of applied voltage. However the curves deviate from this linear behavior at higher values of voltage due to the effect of series resistance and interfacial layer. On increasing the temperature linear region shifts to lower bias voltages. This is due to Richardson's effect as at higher temperatures the carriers can cross the barriers by the smaller voltages at the interface. This is deviation makes this heterojunction diode different from conventional diode, where almost temperature independent *I–V* characteristics were found to exist under forward biasing. The previous studies have reported the similar characteristics for such devices with different interface layers [40–42]. The current transport across such devices can be modeled with the help of thermionic emission theory under bias voltage; *V* as [42–44]:

$$I = I_S \exp\left(\frac{q(V - IR_S)}{\eta kT}\right) \left[1 - \exp\left(\frac{-q(V - IR_S)}{kT}\right)\right] \tag{2}$$

where V is the forward-bias voltage, q is the electron charge, R_S is series resistance, k is the Boltzmann constant, T is the absolute temperature, I_S is reverse saturation current and η is the ideality factor.

The majority carriers are supposed to across the barriers due to thermionic emission according to this theory. The relation between reverse saturation current; I_S and zero bias barrier height; φ_{b0} can be expressed as given below [42–44].

$$I_S = A_d A^{**} T^2 \exp\left(\frac{-q\varphi_{b0}}{kT}\right) \tag{3}$$

where A_d is the contact area, A^{**} is the effective Richardson constant of 3.2×10^5 Am^{-2} K^{-2} for p-Si. Ideality factor is the measure of
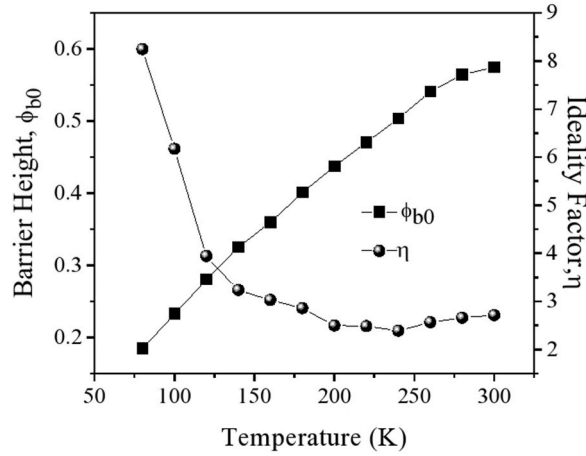
Fig. 5. Barrier height and ideality factor as a function of temperature for Ag/In$_2$O$_3$/p-Si/Al heterojunction diode.
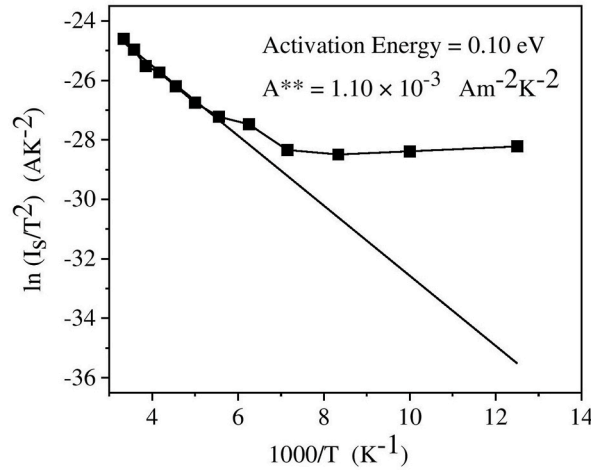

Fig. 6. The activation energy plot of Ag/In$_2$O$_3$/p-Si/Al heterojunction diode.

deviation between *I–V* data obtained from experiment and thermionic emission theory. By employing equation (1) the ideality factor η can be expressed as [42–44]:

$$\eta = \frac{q}{kT} \frac{dV}{d(\ln I)}$$

(4)

The ideality factor is an essential parameter which indicates uniformity in the formation of Schottky barrier. The value of ideality factor for an ideal *p-n* junction is one. From equation (3) the barrier height can be expressed as:

$$\varphi_{b0} = \frac{kT}{q} \ln\left(\frac{A_d A^{**} T^2}{I_s}\right)$$

(5)

from Fig. 5 it was found that the values of φ_{b0} increase and η decrease with the rise in measured temperature.

The temperature dependent values of barrier height φ_{b0} were found to be decrease from 0.57eV to 0.18eV with the decrease in temperature from 300 K to 80 K. This is attributed to the fact that at low temperatures the current conduction is mainly due to the charge carriers which surmount the barriers of lower heights. This indicates the phenomenon of tunneling low temperatures.

The compatibility of pure thermionic emission theory is mainly determined by Ideality factor. The various factors such as thermionic field emission, inhomogeneities, recombination current, image force lowering and the interfacial effects deviate the value of ideality factor from unity [45,46]. Moreover, in heavily doped semiconductor the forward bias current is mainly resulted by the tunneling electrons at low temperature. With rise in the temperature the tunneling of carriers drops and the current obtained can be due to pure thermionic emission theory [46]. The measured ideality factor is possessing relatively small values up to 180 K temperature thereafter increases marginally and then significantly below 120 K acquiring high value of 8.24 at 80 K. This shows that the
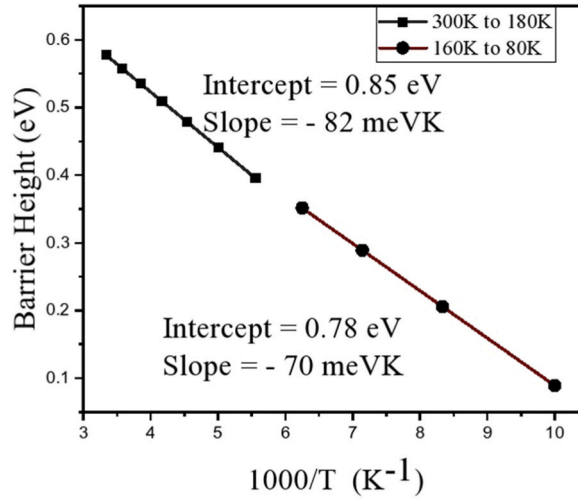
Fig. 7. The apparent barrier height φ_{ap} obtained from *I–V* measurements as a function of inverse temperature.

current transport mechanism deviates from pure thermionic emission theory in the heterojuction Ag/In$_2$O$_3$/*p*-Si/Al due to series resistance. The non-uniformity of the interfacial charges and the inhomogeneity in thickness of grown In$_2$O$_3$ film are also responsible for the observed variations as shown in Fig. 5 [47].

Equation (5) can be rewritten as

$$\ln\left(\frac{I_s}{T^2}\right) = \ln(A_d A^{**}) - \frac{q\varphi_{b0}}{kT} \tag{6}$$

Fig. 6 shows the variation of $\ln\left(\frac{I_s}{T^2}\right)$ vs $\frac{1000}{T}$ which is also known as Richardson's plot and enables us to estimate the effective barrier height by using saturation current density. The assumed Richardson's plot should be a straight line with slope equal to effective barrier height and intercept at the ordinate designates Richardson constant value. But the observed variations are non-linear and which is the consequences of temperature dependant barrier height and ideality factor. From the figure it is evident that the fitting of experimental data in to a straight line is feasible only at higher values of temperature. About 0.10 eV, activation energy and $1.10 \times 10^{-3}\,\mathrm{Am^{-2}K^{-2}}$, Richardson constant were obtained by asymptotic fitting of the experimental data. The obtained value of Richardson constant is much lower than the known value of for *p*-Si; which is $3.2 \times 10^5\,\mathrm{Am^{-2}K^{-2}}$ [48]. This discrepancy is associated with potential fluctuations of the barriers and lateral inhomogeneities at the interface. In fact, the interfacial region of heterojunction is not atomically smooth and flat but rough which results these spatial fluctuations. So the classical thermionic emission theory which demands the existence of single potential at the barrier cannot explain this discrepancy. These undesirable outcomes clearly indicate the deviation from pure thermionic emission mechanism hence to understand the obtained behavior further investigations are required.

2.5. Analysis of barrier height inhomogeneities

The above abnormalities in the barrier height, ideality factor, Richardson's constant can be addressed by using analytical potential fluctuation model with Gaussian distribution of barrier heights due to spatial inhomogeneities at the interface [49]. According to Gaussian distribution of barrier height inhomogeneities with mean barrier height, $\overline{\varphi}_{b0}$ and standard deviation, σ [49], we have the following expression:

$$\varphi_{ap} = \overline{\varphi}_{b\,0} - \frac{q\sigma^2}{2kT} \tag{7}$$

where $\varphi_{ap}, \overline{\varphi}_{b0}, \sigma$ stands for apparent barrier height, mean barrier height and standard deviation respectively. The plot of φ_{b0} against 1000/T shown in Fig. 7 provides the mean barrier height and standard deviation for the Ag/In$_2$O$_3$/*p*-Si/Al heterojunction. Fig. 7 indicates the presence of two straight lines rather than one, with transition occurring at 180 K. These results show the presence of double Gaussian distribution of barrier heights. The slope and intercept of the plot gives $\overline{\varphi}_{b0} = 0.85\,\mathrm{eV}$ and $\sigma = 0.014$ V, respectively in the temperature range 300 K–180 K and $\overline{\varphi}_{b0} = 0.78\,\mathrm{eV}$ and $\sigma = 0.012$ V, respectively in the temperature range 160 K–80 K. Usually, σ corresponds to barrier inhomogeneities and is the evidence of Gaussian distributions of barrier heights at interfacial region of the In$_2$O$_3$/*p*-Si heterojunction. At low temperatures the current transport mechanism is modified by potential fluctuations and Gaussian distributions of barrier heights. Using equations (6) and (7) we get the modified Richardson's relation as:
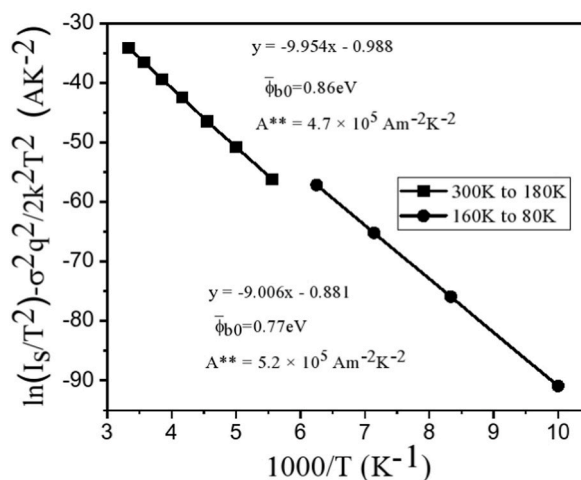
Fig. 8. Modified activation energy plots corresponding to the standard deviations σ = 0.014 V and 0.012 V.

$$\ln\left(\frac{I_S}{T^{2}}\right) - \frac{q^2\sigma^2}{2k^2 T^2} = \ln\ (A_d\ A^{**}) - \frac{q\ \overline{\varphi}_{b0}}{kT} \tag{8}$$

along with original activation energy the variations of modified activation energy $\ln\left(\frac{I_S}{T^2}\right) - \frac{q^2\sigma^2}{2k^2 T^2}$ against 1000/T are illustrated in Fig. 8. The slope and the intercept give the value of $\varphi_{b0} = 0.86$ eV and the Richardson's constant, $A^{**} = 4.7 \times 10^5$ Am^{-2}K^{-2}; respectively in the temperature range 300 K–180 K and $\varphi_{b0} = 0.77$ eV and the Richardson's constant, $A^{**} = 5.2 \times 10^5$ Am^{-2}K^{-2}; respectively in the temperature range 160 K–80 K. The presence of defect states and inhomogeneity at the interface are responsible for double Gaussian distribution of barrier heights. The obtained values of Richardson's constant are close to its real value.

3. Conclusions

The Ag/In$_2$O$_3$/p-Si/Al heterojunction was successfully fabricated by depositing thin films of In$_2$O$_3$ on boron doped silicon wafer with (400) surface orientation using pulsed laser ablation technique. The In$_2$O$_3$ films were found to be nanocrystalline having 56.56 nm grain size. The AFM studies have showed that smooth surface of the film with uniform distribution of grains. The approximate roughness (Rq) of In$_2$O$_3$ film was found to be 1.02 nm. The optical band gap obtained through UV/VIS studies is 3.89 eV. The current transport mechanism of the fabricated device found to possess favorable rectifying behavior in the temperature range 300 K–80 K. From the experimental analysis of current-voltage data it is evident that ideality factor decreases while zero-biased barrier height increases with rising temperature. The temperature dependence of barrier height leads to the non-linearity in activation energy plot and deviation from pure thermionic emission mechanism. By taking into account the interfacial barrier height inhomogeneities along with Gaussian distributions of barrier heights, the temperature dependence of current-voltage characteristics can be successfully explained. The interfacial barrier height inhomogeneities at low temperatures are responsible for the deviation of zero-bias barrier height. The temperature dependence of *I–V* data has revealed the existence of double Gaussian distribution of barrier heights with mean values of 0.85eV and 0.78eV with standard deviation 0.014 V and 0.012 V, respectively. The modified Richardson's plot gives the average barrier height and Richardson's coefficient as 0.86eV and 4.7×10^5 Am^{-2}K^{-2} in the temperature range 300 K–180 K and 0.77eV and 5.2×10^5 Am^{-2}K^{-2}, respectively in the temperature range 160 K–80 K. The values of Richardson's constants are of the order of known theoretical value of 3.2×10^5 Am^{-2} K^{-2}.

Data availability statement

All data generated or analyzed during this study is included in this published article.

Compliance with ethical standards

No funding was received.

Declaration of Competing Interest

I wish to confirm that there are no known conflicts of interest associated with this publication and there has been no significant financial support for this work that could have influenced its outcome.

References

[1] M. Hagerott, H. Jeon, A.V. Nurmikko, W. Xie, D.C. Grillo, M. Kobayashi, R.L. Gunshor, Indium tin oxide as transparent electrode material for ZnSe-based blue quantum well light emitters, Appl. Phys. Lett. 60 (1992) 2825–2827.

[2] E. Gautier, A. Lorin, J.M. Nunzi, A. Schalchli, J.J. Benattar, D. Vital, Electrode interface effects on indium–tin–oxide polymer/metal light emitting diodes, Appl. Phys. Lett. 69 (1996), 1071-1073.

[3] T. Margalith, O. Buchinsky, D.A. Cohen, A.C. Abare, M. Hansen, S.P. Denbaars, L.A. Coldren, Indium tin oxide contacts to gallium nitride optoelectronic devices, Appl. Phys. Lett. 74 (1999), 3930-3332.

[4] R.L. Weiher, R.P. Ley, Optical properties of indium oxide, J. Appl. Phys. 37 (1996) 299–302.

[5] E.B. Ali, H.E. Maliki, J.C. Bernede, M. Sahnoun, A. Khelil, O. Saadane, In$_2$O$_3$ deposited by reactive evaporation of indium in oxygen atmosphere influence of post-annealing treatment on optical and electrical properties, Mater. Chem. Phys. 73 (2002) 78–85.

[6] J.H. Noh, S.Y. Ryu, S.J. Jo, C.S. Kim, S.W. Sohn, P.D. Rack, D.J. Kim, H.K. Baik, Indium oxide thin film transistors fabricated by RF sputtering at room temperature, EEE Electron, Dev. Lett. 31 (2010) 567–569.

[7] A. Ghosh, A. Mondal, A. Das, S. Chattopadhyay, K.K. Chattopadhyay, Removal of oxygen related defects from chemically synthesized In$_2$O$_3$ thin film doped with Er by spin-on technique, J. Alloys Compd.. 695 1260-1265..

[8] Y. Yang, L. Wang, H. Yan, S. Jin, T.J. Marksa, S. Li, Highly transparent and conductive double-layer oxide thin films as anodes for organic light-emitting diodes, Appl. Phys. Lett. 89 (2006), 051116.

[9] M.A. Majeed, W. Khan, M. Ahamed, M. Alhoshan, Structural and optical properties of In2O3 nanostructured thin film, Mater. Lett. 79 (2012) 119–121.

[10] D. Beena, K.J. Lethy, R. Vinod Kumar, A.P. Detty, V.P. Mahadevan pillai, V. Ganesan, Photoluminescence in laser ablated nanostructured indium oxide thin films, Optoelectron. Adv. Mater.- Rapid Commun. 5 (2011) 1–11.

[11] W. Miao, X. Li, Q. Zhang, L. Huang, Z. Zhang, L. Zhang, X. Yan, Transparent conductive In2O3: Mo thin films prepared by reactive direct current magnetron sputtering at room temperature, Thin Solid Films 500 (2006) 70–73.

[12] X. Xiu, Z. Pang, M. Lv, Y. Dai, L. Ye, S. Han, Transparent conducting molybdenum-doped zinc oxide films deposited by RF magnetron sputtering, Appl. Surf. Sci. 253 (2007) 3345–3348.

[13] A. Subrahmanyam, U.K. Barik, Synthesis of *p*-type transparent conducting silver indium oxide (AIO) thin films by reactive electron beam evaporation technique, J. Phys. Chem. Solid. 66 (2005) 817–822.

[14] S. Sun, J. Huang, D. Lii, Effects of H$_2$ in Indium-Molybdenum oxide films during high density plasma evaporation at room temperature, Thin Solid Films 6 (2004) 469–470.

[15] Y. Meng, X. Yang, H. Chen, J. Shen, Y. Jiang, Z. Zhang, Z. Hua, A new transparent conductive thin film In$_2$O$_3$: Mo, Thin Solid Films 394 (2001) 218–222.

[16] J.H. Lee, S.Y. Lee, B.O. Park, Fabrication and characteristics of transparent conducting In2O3–ZnO thin films by ultrasonic spray pyrolysis, Mater. Sci. Eng. 127 (2006) 267–271.

[17] I. Shim, C. Kim, Doping effect of indium oxide-based diluted magnetic semiconductor thin films, J. Magn. Magn Mater. E1571 (2004) 272–276.

[18] J. Hu, R.G. Gordon, Textured aluminum-doped zinc oxide thin films from atmospheric pressure chemical-vapor deposition, J. Appl. Phys. 71 (1992) 880–890.

[19] R.K. Gupta, K. Ghosh, R. Patel, P.K. Kahol, Effect of thickness on optoelectrical properties of Mo-doped indium oxide films, Appl. Surf. Sci. 255 (2008) 3046–3048.

[20] K. Arshak, O. Korostynska, J. Henry, Thick film PN-junctions based on mixed oxides of indium and silicon as gamma radiation sensors, Microelectron. Int. 21 (2004) 19–27.

[21] R.K. Gupta, F. Yakuphanoglu, Analysis of device parameters of Al/In$_2$O$_3$/*p*-Si Schottky diode, Microelectron. Eng. 105 (2013) 13–17.

[22] R.A. Ismaila, D.N. Raouf, D.F. Raouf, High efficiency In$_2$O$_3$/c-Si heterojunction solar cells produced by rapid thermal oxidation, J. Optoelectron. Adv. Mater. 8 (2006) 1443–1446.

[23] E. Savarimuthu, K.C. Lalithambika, A. Moses Ezhil Raj, L.C. Nehru, S. Ramamurthy, A. Thayumanavan, C. Sanjeeviraja, M. Jayachandran, Synthesis and materials properties of transparent conducting In$_2$O$_3$ films prepared by sol–gel-spin coating technique, J. Phys. Chem. Solid. 68 (2007) 1380–1389.

[24] Z.X. Cheng, X.B. Dong, Q.Y. Pan, J. Zhang, X.W. Dong, Preparation and characterization of In$_2$O$_3$ nanorods, Mater. Lett. 60 (2006) 3137–3140.

[25] S. Kaleemulla, A.S. Reddy, S. Uthanna, P.S. Reddy, Physical properties of flash evaporated In2O3 films prepared at different substrate temperatures, Mater. Lett. 61 (2007) 4309–4313.

[26] S. Bhuvaneswari, M. Seetha, J. Chandrasekaran, R. Marnadu, High photoresponsive p-Si/n-In$_2$O$_3$ junction diodes with low ideality factor prepared using closely packed octahedral structured In$_2$O$_3$ thin films, J. Inorg. Organomet. Polym. Mater. 30 (2020) 4552–4568.

[27] H. von Wenckstern, D. Splith, F. Schmidt, M. Grundmann, O. Bierwagen, J.S. Speck, Schottky contacts to In$_2$O$_3$, Apl. Mater. 2 (2014), 046104.

[28] A.F. Ozdemir, A. Turut, A. Kokce, The double Gaussian distribution of barrier heights in Au/n-GaAs Schottky diodes from I–V –T characteristics, Semicond. Sci. Technol. 21 (2006) 298–302.

[29] A. Turut, On current-voltage and capacitance-voltage characteristics of metal-semiconductor contacts, Turk. J. Phys. 44 (2020) 302–347.

[30] F.M. Coşkun, O. Polat, M. Coşkun, A. Turut, M. Caglar, Z. Durmus, H. Efeoglu, Temperature dependent current transport mechanism in osmium-doped perovskite yttrium manganite-based heterojunctions, J. Appl. Phys. 125 (2019), 214104.

[31] I. Orak, A. Kocyigit, S. Karatas, The analysis of the electrical and photovoltaic properties of Cr/*p*-Si structures using current-voltage measurements, Silicon 10 (2018) 2109–2116.

[32] S. Karatas, M. Cakar, Temperature dependence of the electrical and interface states of the Sn/Rhodamine-101/*p*-Si Schottky structures, Synth. Met. 159 (2009) 347–351.

[33] S. Karatas, Comparison of electrical parameters of Zn/*p*-Si and Sn/*p*-Si Schottky barrier diodes, Solid State Commun. 135 (2005) 500–504.

[34] O. Demircioglu, S. Karatas, N. Yıldırım, O.F. Bakkaloglu, Effects of temperature on series resistance determination of electrodeposited Cr/n-Si/Au–Sb Schottky structure, Microelectron. Eng. 88 (2011) 2997–3002.

[35] F. Hossein-Babaei, M.M. Lajvardi, N. Alaei-Sheini, The energy barrier at noble metal/TiO$_2$ junctions, Appl. Phys. Lett. 106 (2015), 083503.

[36] J.S. Jeong, Y.H. Kim, J.Y. Lee, Morphology and structure of nano-sized In$_2$O$_3$ crystals synthesized by wet reaction, J. Kor. Phys. Soc. 42 (2003) S254–S257.

[37] Y. Ishikawa, Y. Matsumoto, Electrodeposition of TiO$_2$ photocatalyst into nano-pores of hard alumite, Electrochim. Acta 46 (2001) 2819–2824.

[38] J. Tauc, F. Abeles, Optical Properties of Solids, North-Holland Amsterdam, 1971.

[39] M.A.M. Khan, W. Khan, M. Ahamed, M. Alhoshan, Structural and optical properties of In$_2$O$_3$ nanostructured thin film, Mater. Lett. 79 (2012) 119–121.

[40] S. Chand, J. Kumar, On the existence of a distribution of barrier heights in Pd$_2$Si/Si Schottky diodes, J. Appl. Phys. 80 (1996) 288–294.

[41] O. Pakma, C. Tozlu, N. Kavasoglu, S. Kavasoglu, S. Ozden, I–V–T analysing an inhomogeneous Au/Poly(4-vinyl phenol)/*p*-Si structure with a double Gaussian distribution of barrier heights, J. Sol. Gel Sci. Technol. 58 (2011) 244–250.

[42] O. Pakma, N. Serin, T. Serin, Ş. Altındal, The double Gaussian distribution of barrier heights in Al/TiO$_2$/*p*-Si (metal-insulator-semiconductor) structures at low temperatures, J. Appl. Phys. 104 (2008), 014501.

[43] S.M. Sze, K.K. Ng, Physics of Semiconductor Devices, Wiley, New Jersey, 2007.

[44] E.H. Rhoderick, R.H. Williams, Metal Semiconductor Contacts, Clarendon Press, Oxford, 1988.

[45] J. Osvald, T. Lalinsky, G. Vanko, High temperature current transport in gate oxides based (GaN)/AlGaN/GaN Schottky diodes, Appl. Surf. Sci. 461 (2018) 206–211.

[46] R.T. Tung, Recent advances in Schottky barrier concepts, Mater. Sci. Eng. R. 35 (2001) 1–138.

[47] M.H. Suhail, G.M. Rao, S. Mohan, Dc reactive magnetron sputtering of titanium-structural and optical characterization of TiO$_2$ films, J. Appl. Phys. 71 (1992) 1421–1427.

[48] R. Kumar, S. Chand, Fabrication and electrical characterization of nickel/*p*-Si Schottky diode at low temperature, Solid State Sci. 58 (2016) 115–121.

[49] J.H. Werner, H.H. Güttler, Barrier inhomogeneities at Schottky contacts, J. Appl. Phys. 69 (1991) 1522–1533.